Sedimentation to form rough, quasi-one-dimensional interfaces

M. L. Kurnaz and J. V. Maher
Department of Physics and Astronomy, University of Pittsburgh, Pittsburgh, Pennsylvania 15260
(Received 20 March 1995; revised manuscript received 15 September 1995)

The quasi-two-dimensional sedimentation of silica particles in viscous fluids results in quasi-one-dimensional rough surfaces. These surfaces are rough on all length scales between the particle size and the cell size, but different roughness exponents are observed in two well defined length-scale regimes. The range of hydrodynamic forces should play an important role in determining which, if either, length-scale regime shows universal properties. The strong similarity between the height-height correlations of the surface and the density-density correlations inside the flow at longer length scales suggests that the roughness at longer length scales is very closely tied to the hydrodynamic interactions in the fluid. Measurements have been performed at three different cell aspect ratios and at three different fluid viscosities and in no case is there an observable change in the crossover length scale of the system.

PACS number(s): 81.15.Lm, 47.15.Gf, 47.53.+n, 05.40.+j

I. INTRODUCTION

The growth of rough surfaces is a problem of practical importance and also involves fundamental nonequilibrium statistical physics [1]. Although sedimentation has been widely investigated in various areas of geology and engineering, the formation of rough interfaces via sedimentation is still relatively unstudied [2]. The hydrodynamics of this problem is very complicated and should involve long-range forces caused by backflows from the motion of neighboring particles out to a distance set by viscosity and the density of the particles in the settling suspension [3,4]. Since hydrodynamic forces are in principle long range, rough interfaces formed through sedimentation provide a significantly different growth situation for comparison with other studies of apparently similar final interfaces. The similarity of rough interfaces grown through such different mechanisms leads to the question of the possible existence of universal phenomena, and if sedimentation fits into a class exhibiting universal phenomena, can one use noise plus a simple growth law to explain them? In this paper we report experiments in which several control parameters (fluid viscosity, sedimentation cell width, and cell length) were varied to examine the robustness and possible asymptotic features of quasi-one-dimensional interfaces formed by quasi-two-dimensional sedimentation.

II. EXPERIMENTAL METHOD

In the sedimentation experiment discussed in this paper all measurements have been performed with closed cells. The walls of these cells are of 1/4-in. float glass and these are held 1 mm apart by sealed side frames of precision-machined Plexiglass. To examine the effects of viscosity, each cell was filled with one of three different viscous liquids. A very large number ($\sim 40\,000$) of 0.06-cm-diam monodisperse silica spheres [5] were also placed in the cells before they were closed; these particles filled approximately 1–3 % of the volume of the cells. The various cell sizes used and corresponding liquids are given in Table I. One typical cell is shown in Fig. 1. Each cell could be rotated about a horizontal axis perpendicular to the gap direction. When the cell was rotated, the particles that had been at rest at the bottom fell through the oil, slowly building a new surface at the bottom of the cell. During each such process we photographed the cell (or parts of the cell). All of our measurements were made with a 35-mm single-lens reflex slide camera. The slides were then digitized to a maximum resolution of 2048×1366 pixels by a Nikon LS 3500 35-mm film scanner. Individual particles were typically resolvable and thus the position of the particles could be traced very accurately using the image analysis program OPTIMAS [6].

We concentrated our efforts mainly on analyzing the final surface and the dynamics of its formation. The analysis of the final interface (after all the particles have come to rest) is usually more accurate than the analysis made during the formation of the interface, because the

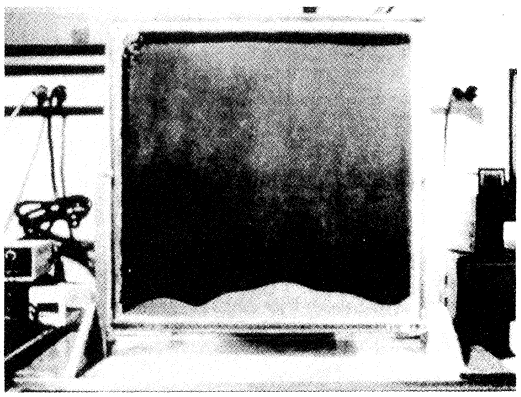

FIG. 1. Example of a typical cell with dimensions of 40×40 cm^2 and a cell gap of 1 mm.

TABLE I. Various cell sizes used in the sedimentation experiment and corresponding liquids.

Cell	Size (cm^2)	Filling liquid	α_s	α_l	β
A	40×40	glycerin (1300 cP)	0.80 ± 0.05	0.93 ± 0.03	0.47 ± 0.13
B	40×40	heavy oil (180 cP)	0.76 ± 0.07	0.90 ± 0.06	0.43 ± 0.18
C	40×40	light oil (50 cP)	0.72 ± 0.03	0.93 ± 0.04	0.46 ± 0.03
D	40×20	heavy oil (180 cP)	0.79 ± 0.04	0.94 ± 0.04	0.60 ± 0.02
E	120×30	heavy oil (180 cP)	0.85 ± 0.06	0.97 ± 0.03	0.66 ± 0.10

motion of the individual particles at earlier stages of the process tends to blur the image obtained and also because it can be ambiguous whether a particular particle has joined the interface or is still falling. Particle density fluctuations in the fluid above the interface could also be determined from the intensity distribution in the digitized photographs, with intensity vs position typically extracted for several horizontal lines defined on the image of the cell.

Although there is convection in the cell at large scales during the flow, as particles join the interface they tend to settle in gently on a vertical line with no obvious lateral movement as they approach the surface. After hitting the interface they roll to the nearest local minimum, which is no more than one particle diameter away from the impact point. Since they roll to the nearest local minimum, overhangs are never formed.

For each cell type we have measured several time series in which patterns were measured at regular intervals from the earliest completely covering array until the last of the particles settled down. We have also measured numerous independent runs in which we measured only the final configuration of the settled particles.

The first obvious question about the global behavior of the settling particles is whether the final configuration of particles might depend in some very important way on the initial configuration of particles at the top of the cell. We found that, if we tilted and shook the cell to force an initial configuration of particles that was very atypical, then the system required approximately four resettlings of the particles before the atypical configuration's features were completely obliterated. However, if the initial configuration was not prepared to be atypical, no obvious correlation between initial and final configurations could be discerned by eye, as can be seen in Fig. 2.

In an attempt to make this insight quantitative and to look for subtler correlations, we defined a mean absolute difference function [7] between initial and later configurations to be

$$\Delta h_n = \frac{1}{N} \sum_{x_i} | h_n(x_i) - h_1(x_i) | , \qquad (1)$$

where n is the number of the configurations in the sequence, $h_n(x_i)$ is the height of the interface at horizontal position x_i after the nth run, and N is the number of surface sites x_i. Figure 3 shows this function for 50 sedimentation runs following a very atypical configuration in which the particles formed a triangle on one side of the cell. Figure 4 shows data from most of the same runs, but the sixth run from Fig. 3 is used as the initial configuration and compared with all subsequent runs. No obvious correlations appear once the triangular configuration is forgotten by the system.

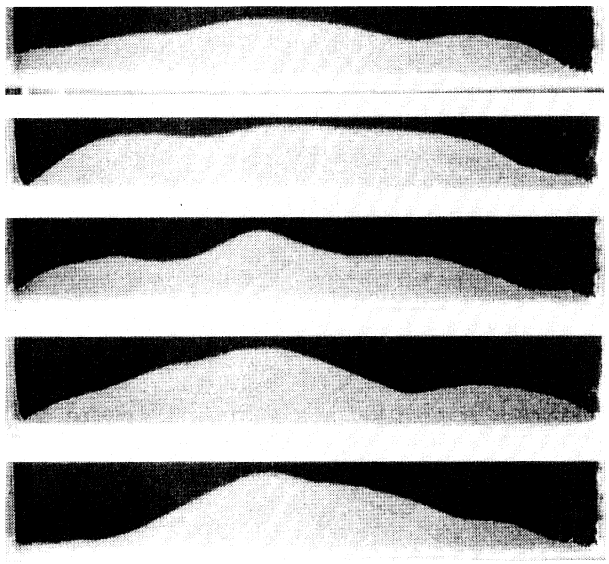

FIG. 2. Evolution of a typical initial configuration. Starting from the top picture, each picture shows the final interface after the cell is rotated once. The data shown are for cell type A.

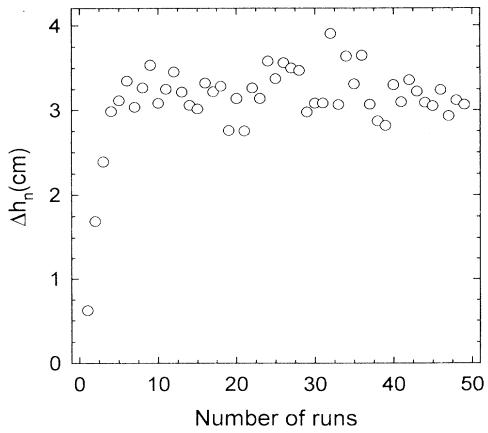

FIG. 3. Mean absolute difference function defined in the text using an atypical triangular initial configuration for the first run.

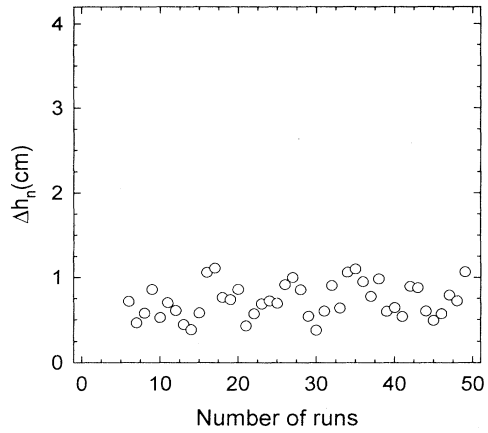

FIG. 4. Mean absolute difference function defined in the text using a typical initial configuration for the first run.

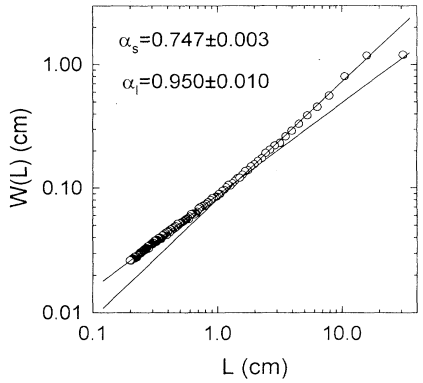

FIG. 6. Example of the roughness function $W(L,t)$ at the end of a typical run for cell type A.

If we go back to Fig. 2, which is a collection of several typical configurations at the end of sedimentation runs, we see that there was a strong tendency to have minima near the walls of the cell, so to minimize the wall effects we have only used the middle 70% of each interface for the analyses presented below. Within the middle 70% of the cell there is, on the average, only a gentle variation of surface height across the cell. Figure 5 shows the average position of the middle 30 cm of the interface at the end of a run for cell type A, which had a width of 40 cm; this average has been constructed using 46 runs, excluding the atypical, triangular run and its first few descendants at the beginning of the experiment. This issue will be discussed below in greater detail.

The set of final configurations of all the runs from all the cell types can be used to define the roughness of the interface with great accuracy. We define the rms thickness of the interface to be

$$W(L,t) = \left[\frac{1}{N}\sum_{i=1}^{N}\tilde{h}(x_i,t)^2\right]^{1/2}, \tag{2}$$

where

$$\tilde{h}(x_i,t) = h(x_i,t) - \bar{h}(t) \tag{3}$$

and

$$\bar{h}(t) = \frac{1}{N}\sum_{i=1}^{N} h(x_i,t). \tag{4}$$

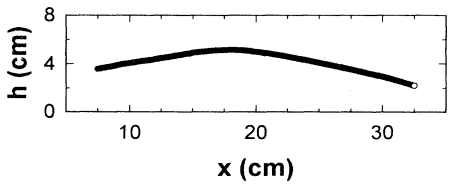

FIG. 5. Interface height as a function of position x averaged over 46 independent final configurations. As discussed in the text, 7.5 cm have been eliminated on each side of the cell.

It is not at all clear that our system is in a scaling regime, nor is it obvious that scaling ideas should apply to sedimentation, but a useful way of analyzing our data is to adopt and extend the standard roughness analysis by tentatively accepting a scaling ansatz for rough interface growth [8]. If we follow this ansatz, we write

$$W(L,t) = L^{\alpha} f(t/L^{\alpha/\beta}), \tag{5}$$

where the exponents α and β are the static and dynamic scaling exponents. The function $f(t/L^{\alpha/\beta})$ is expected to have an asymptotic form such that

$$\begin{aligned} W(L,t) &\sim t^{\beta} \quad \text{for } t \ll L^{\alpha/\beta}, \\ W(L,t) &\sim L^{\alpha} \quad \text{for } t \gg L^{\alpha/\beta}. \end{aligned} \tag{6}$$

Figure 6 shows a typical example of $W(L)$ at late times for cell type A. There are clearly two domains of roughness. At small length scales ($L \leq 1$ cm), there is roughly a decade in L wherein the data appear to follow a power law whose exponent is $\alpha_s = 0.747$ for this final state. At longer length scales ($L \geq 1$ cm), there is roughly a decade over which a different exponent can be identified. The value of this exponent α_l in Fig. 6 is 0.950. As can be seen from Table I, which shows average exponents for all runs in each kind of cell, similar behavior is observed for all cell configurations. Even though it is clear that there cannot be two asymptotic regimes (and there may not be even one), these two well defined roughness regimes are a clear property of our sedimentary interfaces (and of some other experiments on rough interfaces). We will thus proceed to discuss the empirical analysis, postponing interpretation of possible universal effects.

In an attempt to observe early stages of the developing interface and study the dynamics of interface growth, time series of measurements were performed for various flow realizations. Results from one such flow realization can be seen in Fig. 7, where we show the interfacial roughness $W(L,t)$ for three different times in the same run. In Fig. 8 we show the two roughness exponents for all times in the same time series. While the final interface rough-

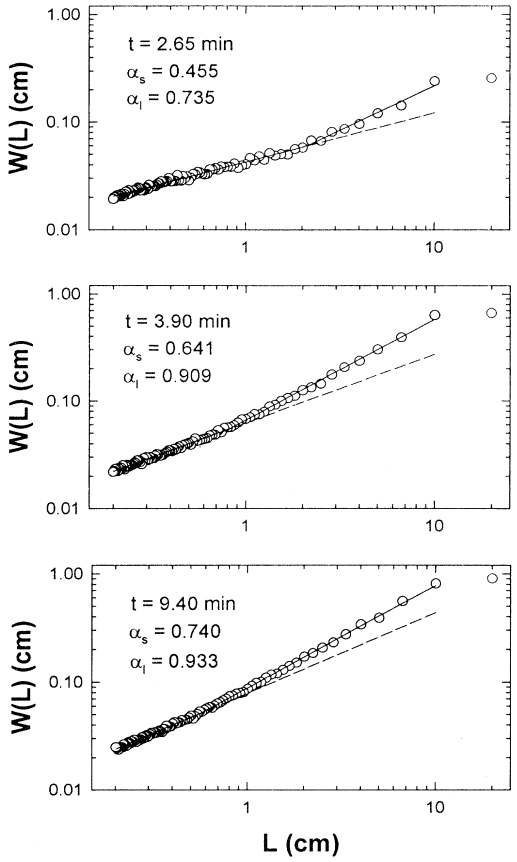

FIG. 7. Roughness function $W(L,t)$ is shown for three values of time in one typical time series for a cell type E.

ness is very reproducible, at the early stages of interface growth, large fluctuations of roughness were observed.

We are aware that in order to apply the preceding scaling analysis to the sedimentation problem, the ensemble average of the height of the interface (Fig. 5) must be a horizontal line. In order to see the effects of the inhomogeneity (departure from horizontal) on our results we have used different averaging methods. The first method is to reference the height to the ensemble average of the type shown in Fig. 5 and not to the average height of a single run. Figure 9 shows one example of this analysis where we have used the same data set that was used to obtain Fig. 6. As can be seen from Fig. 9 the fundamental behavior of the exponents did not change. Through all of the data that has been analyzed the fluctuation in the exponents remained of the order of the fluctuations from one run to the next.

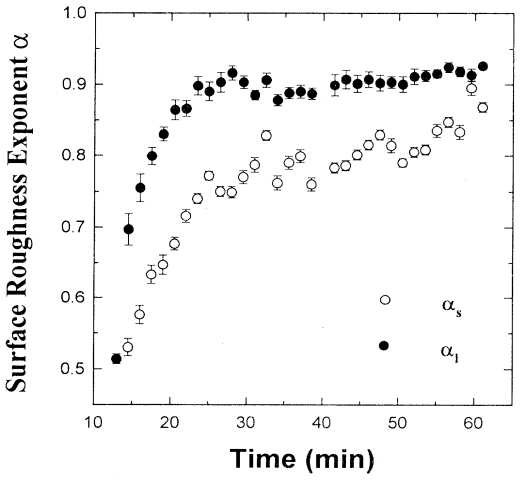

FIG. 8. Time evolution of the two exponents α_s and α_l for a typical time series for cell type A.

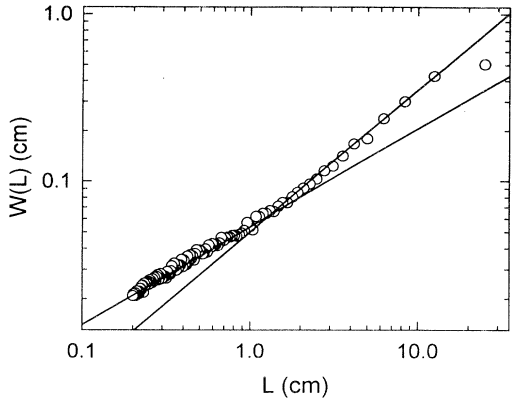

FIG. 9. Example of the roughness function $W(L,t)$ at the end of a typical run for cell type A, where we have referenced the height of the interface to the ensemble average of the 46 runs discussed above and not to the average height of a single run. The two exponents obtained from this plot are $\alpha_s = 0.64$ and $\alpha_l = 0.83$.

We have also investigated the effect of obtaining data from different parts of the final interface, i.e., closer to the walls or from the middle. For this purpose we have divided the interface into smaller boxes of width 10 cm. These boxes were from 0 to 10 cm, from 5 to 15 cm, from 10 to 20 cm, etc. Figure 10 shows this analysis for the average of six runs from the set of 46 final runs for cell type A. The fluctuation in the exponents is small and of the order of the fluctuations from one run to the next.

Another possibility would be to use only data from the center region of the cells used. To investigate this possibility further we have decreased the portion that we have been using in our analysis from 70% to 25% and we have not observed any behavioral change that would suggest an additional advantage of using a smaller (than 70%) portion of the width of the cell in our analysis. All these different averaging techniques convinced us that the data analysis method we are using to describe our results is robust and any changes in averaging will not change the fundamental results discussed in this paper.

Since roughness and correlation analyses might be expected to bring out very different features of a data set of finite size, we have also constructed the height-height correlation function

$$c(L,t) = \langle [\tilde{h}(x',t') - \tilde{h}(x'+L,t'+t)]^2 \rangle_{x',t'}. \qquad (7)$$

Returning to the scaling ansatz of Family and Vicsek [8],

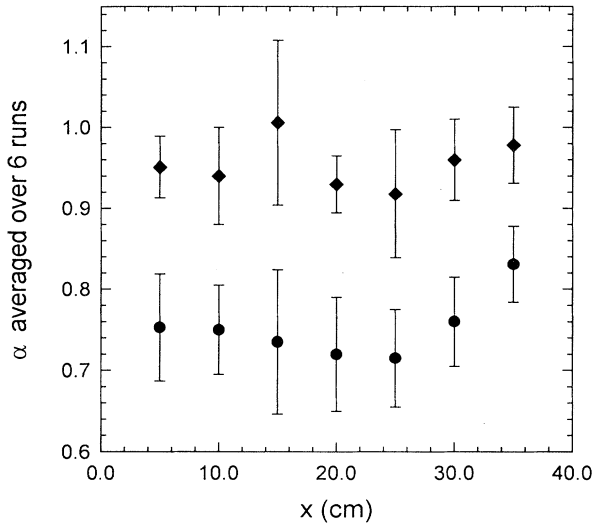

FIG. 10. Roughness exponents α_s and α_l calculated from the data from different parts of the cell in the same run. This figure shows the average final frame behavior over six runs arbitrarily selected from a pool of 46 runs for cell type A. All of the values correspond to analyses of 10-cm intervals with the center point of each interval shown as position x in the cell.

we expect $c(L,0) \sim L^{2\alpha}$ for L significantly less than the length of the cell and $c(0,t) \sim t^{2\beta}$ for short time differences. This approach provides an alternative weighting of the data to determine average exponents. $c(L,0)$ vs L does not always yield roughness exponent values consistent with the previous analysis. This appears to result from the effect discussed above where the roughness exponents change with time and show large fluctuations at early times. If this were not true, then the short-length-scale exponent would in principle be extractable.

In Fig. 11 we show $c(0,t)$ vs t for one time series of cell type A. The value of β determined from Fig. 11 is 0.61 ± 0.05. Table I lists β values for all the time series runs of different cell types. As can be seen in the uncertainties from the table, the value of β fluctuates significantly from run to run, but over all of the runs we obtain an average of $\beta = 0.52 \pm 0.10$. It was not possible to use Eq. (7) to extract reliable values of β from the roughness functions because the analysis is too sensitive to the observed temporal variations in α.

Having used a scaling ansatz to organize the data, we return to the question of which, if either, length-scale regime is the scaling regime. One might argue that the long-length-scale roughness is dominated by wall effects (although the results of Fig. 10 argue against this) and that the short length scales are the ones that exhibit universal effects. On the other hand, hydrodynamic effects are long range, and it might be argued that universal roughening effects would only be expected at spatial separations large enough for the screening effects of many particles to destroy any hydrodynamic coherence. In an attempt to discriminate between these two arguments, we have varied our control parameters to change characteristic length scales of either the apparatus or the particle interactions. That is, we have varied the viscosity and the aspect ratio. While, in principle, changing the viscosity and changing the aspect ratio can be argued to be equivalent, cooperative screening effects in this system are very likely to separate the two effects. Despite our changing the viscosity by changing fluids and the aspect ratio by changing both the length and the width of the cell independently, we found that the short- and long-length-scale roughness exponents remained unchanged (see Table I). The crossover regime at about $L = 1$ cm did not change either, even though it should move toward the wall in a wider cell if long length scales are dominated by cell effects, toward the wall without a change of cell size when viscosity is increased if it arises from the range of hydrodynamic forces, etc. Something is clearly very robust in the form of these random interfaces.

In an attempt to quantify the noise in the problem we have constructed a spatiotemporal fluctuation function [9]

$$\eta(x,t_1) = \frac{\tilde{h}(x,t_2) - \tilde{h}(x,t_1)}{\bar{h}(t_2) - \bar{h}(t_1)}, \tag{8}$$

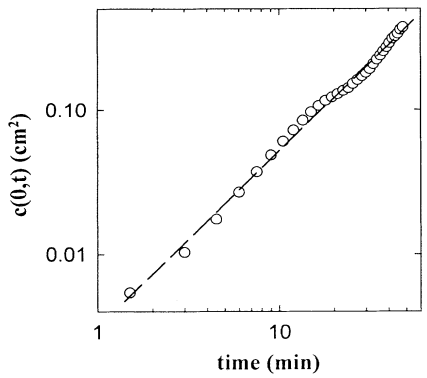

FIG. 11. Height-height correlation function $c(0,t)$ vs t for one time series for cell type A.

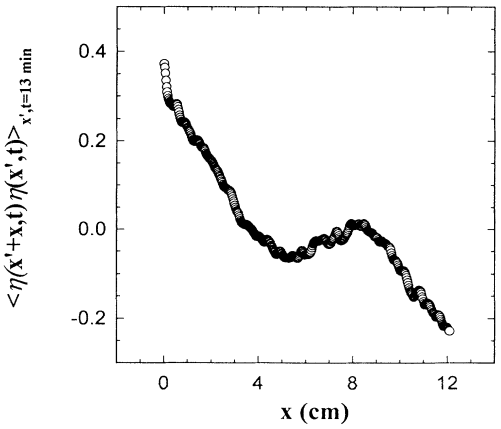

FIG. 12. Spatial correlation function of spatiotemporal fluctuation function $\eta(x,t)$ for arbitrarily chosen $t = 13$ min in one time series of cell type A.

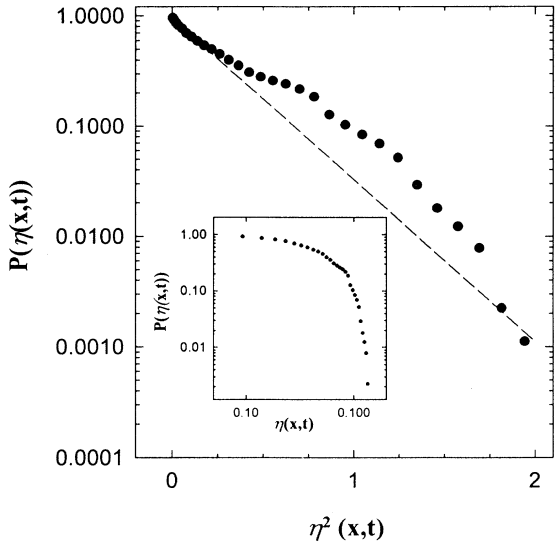

FIG. 13. Probability distribution function of spatiotemporal fluctuation function $\eta(x,t)$ for arbitrarily chosen $t = 13$ min in one time series of cell type A.

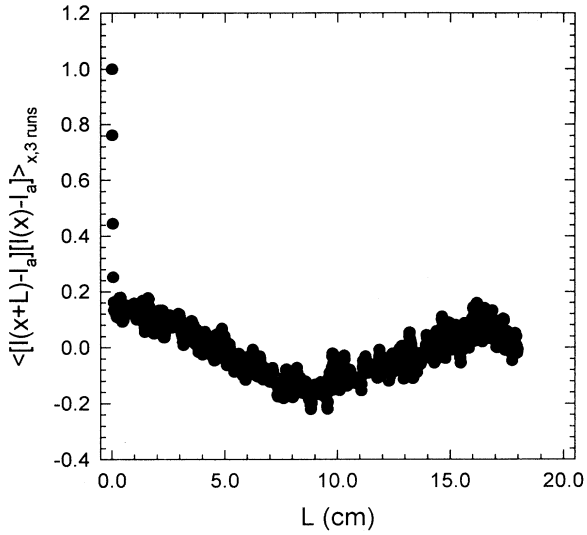

FIG. 15. Density-density correlation function of sedimenting silica spheres in glycerin 6 cm above a bottom of the cell, 25 min after the first particle has reached the bottom. The data shown are the average of three runs.

where t_2 is larger than t_1 by a specified small amount δt. An example of such a spatial correlation function $\eta(x,t)$ is shown in Fig. 12. The noise falls off at short length scales, with a characteristic distance of approximately 2 cm, and is anticorrelated at large length scales (≥ 4 cm). The probability distribution of fluctuations is shown in Fig. 13 vs η^2. If the noise were pure Gaussian, the data in Fig. 13 would fall on a straight line. While the data do not fall on a line, they definitely do not follow a power law (see inset to Fig. 13) and might be considered to be Gaussian with some superimposed long-range distribution.

During all of the runs we have observed complex patterns within the flow far above the interface while the particles are settling down. This leads us to question whether the correlations in the flow may be in some way connected to the spatial correlations in the surface. To investigate this connection we measured the spatial correlation function of the fluctuation of the height of the surface $\tilde{h}$. Figure 14 shows this spatial correlation function averaged over three runs of cell type A. We also obtained the density of particles inside the flow from the reflected light intensity as a function of position, and Fig. 15 shows the density-density correlation function for particles 6 cm above the interface in this cell, averaged over the same three runs. Different cell types at different stages of the flow and at different heights give similar results to the case shown in Fig. 15. The first few points at short length scales come from the self-correlations of the particles and can be ignored. Comparing Fig. 14 with Fig. 15, we can conclude that there are similarities between flow correlations and surface structure correlations at long length scales, but there are no obvious similarities at shorter length scales. The difference in concavity between the two correlation functions at shorter length scales can be seen in Fig. 16, where we have contracted and superimposed the spatial correlation function of Fig. 14 on the density-density correlation function of Fig. 15. This suggests that hydrodynamics may dominate the formation of the long-length-scale roughness, but not the short-scale effects.

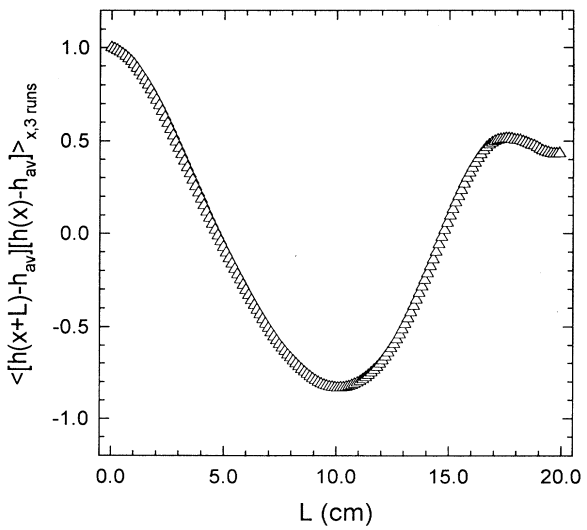

FIG. 14. Spatial correlation function of the fluctuation of the final height of the surface $\tilde{h}$ for cell type A. The figure shows the average over three runs.

Many observers see two different roughness regimes [10–20], and some of them argue that they know which regime is asymptotic. Our inability to change the crossover length scale either by changing the width of the cell (which might be expected to exhibit any important wall effects) or by changing fluid viscosity (which might be expected to change the effective range of particle-particle interactions) leaves us unable to choose which, if

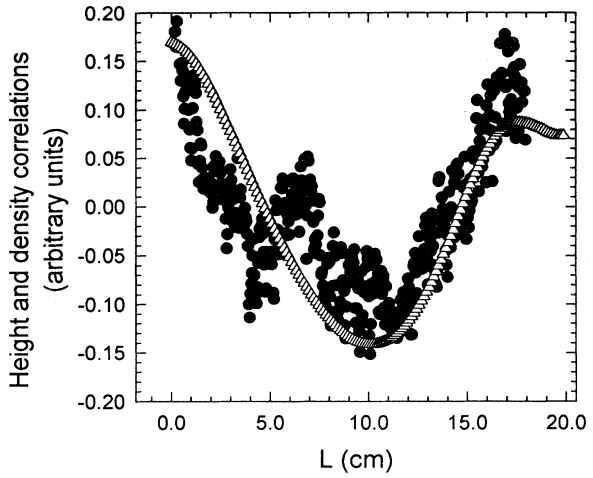

FIG. 16. Spatial correlation function of the fluctuation of final height of the surface (△) and the density-density correlation function of the particles 6 cm above a bottom of the cell (•) are shown. The scale of the vertical axis is arbitrarily adjusted to be able to show the similarities and the differences between the two correlation functions.

either, regime to call asymptotic. On the other hand, the robustness of the results suggests that there are universal aspects to the growth of these sedimentary surfaces, and the lack of change when cell length is drastically increased argues against the surfaces exhibiting transient effects.

Unfortunately, it is difficult to comment on the role of hydrodynamics when we have so many particles settling simultaneously. Analytic sedimentation theory has succeeded only in analyzing the attraction between two settling particles [21], the effective behavior of settling particles in the dilute regime [3,22,23], and some features of many-body interactions between the particles [24,25]. Computer simulations have proven to be quite successful in accounting for interactions among hundreds (but not yet tens of thousands) of particles [26]. In addition, phenomenological analytic theory has described some interesting length scales that appear in the breakup of a line or a plane of settling homogeneous particles [27,28] or of arrays of mixed particles [29]. Beyond this, some recent theoretical work [30,31] has heightened pessimism by highlighting how complicated the situation is, while interesting experimental results have become available and other recent theoretical work [4,32] holds out some hope of determining the particles' interactions and profiles through wide ranges of volume fraction and Péclet number in sedimentation problems.

III. CONCLUSION

Surface roughness in sedimentation is robust against a series of significant changes in control parameters of fluid flow and this suggests that the roughness may represent universal behavior. However, there cannot be two asymptotic regimes and there is clearly more to be understood in the double-regime phenomena of this problem. It is nevertheless worth noting that if the large L regime is asymptotic, then the correlations with the fluid flow suggest that we look to the hydrodynamics for an explanation. If the small L regime is asymptotic, surface fluctuations do not correlate closely with density fluctuations in the supernatant fluid and then a simple growth law plus noise might be appropriate to explain the results we obtained (and the noise we measure is close to Gaussian). If the latter approach were to be adopted, it would raise the same question raised by several other rough interface growth experiments that the roughness exponents are not those expected from the Kardar-Parisi-Zhang dynamics [33] with Gaussian noise [7,34,35].

ACKNOWLEDGMENTS

We appreciate helpful discussions with F. Family and D. Jasnow. We are grateful to D. Bideau for giving us samples of monodisperse silica particles. This work is supported by the U.S. DOE Grant No. DE-FG02-84ER45131.

[1] F. Family and T. Vicsek, *Dynamics of Fractal Surfaces* (World Scientific, Singapore, 1991).
[2] M. L. Kurnaz, K. V. McCloud, and J. V. Maher, Fractals **1**, 1008 (1993).
[3] R. H. Davis and A. Acrivos, Annu. Rev. Fluid. Mech. **17**, 91 (1985).
[4] F. M. Auzerais, R. Jackson, and W. B. Russel, J. Fluid Mech. **195**, 437 (1988).
[5] D. Bideau (private communication).
[6] BIOSCAN OPTIMAS Version 3.01, BioScan Inc., Edmonds, WA.
[7] J. G. Amar and F. Family, Phys. Rev. E **47**, 1595 (1993).
[8] F. Family and T. Vicsek, J. Phys. A **18**, 75 (1985).
[9] V. K. Horvath, F. Family, and T. Vicsek, Phys. Rev. Lett. **67**, 3207 (1991).
[10] P. Pfeifer, Y. J. Wu, M. W. Cole, and J. Krim, Phys. Rev. Lett. **62**, 1997 (1989).
[11] M. Matsushita and S. Ouchi, Physica D **38**, 246 (1989).
[12] V. K. Horvath, F. Family, and T. Vicsek, J. Phys. A **24**, L25 (1991).
[13] E. A. Eklund, R. Bruinsma, J. Rudnick, and R. S. Williams, Phys. Rev. Lett. **67**, 1759 (1991).
[14] P. Herrasti, P. Ocon, L. Vazquez, R. C. Salvarezza, J. M. Vara, and A. J. Arvia, Phys. Rev. A **45**, 7440 (1992).
[15] R. C. Salvarezza, L. Vazquez, P. Herrasti, P. Ocon, J. M. Vara, and A. J. Arvia, Europhys. Lett. **20**, 727 (1992).
[16] S. V. Buldyrev, A. L. Barabasi, F. Caserta, S. Havlin, H. E. Stanley, and T. Vicsek, Phys. Rev. A **45**, R8313

(1992).
[17] M. A. Cotta, R. A. Hamm, T. W. Staley, S. N. G. Chu, L. R. Harriott, M. B. Panish, and H. Temkin, Phys. Rev. Lett. **70**, 4106 (1993).
[18] W. M. Tong, R. S. Williams, A. Yanase, Y. Segawa, and M. S. Anderson, Phys. Rev. Lett. **72**, 3374 (1994).
[19] L. Vazquez, R. C. Salvarezza, P. Ocon, P. Herrasti, J. M. Vara, and A. J. Arvia, Phys. Rev. E **49**, 1507 (1994).
[20] T. Engoy, K. J. Maloy, A. Hansen, and S. Roux, Phys. Rev. Lett. **73**, 834 (1994).
[21] J. Happel and H. Breuner, *Low Reynolds Number Hydrodynamics* (Prentice-Hall, Englewood Cliffs, NJ, 1965).
[22] G. K. Batchelor, J. Fluid Mech. **119**, 379 (1982).
[23] W. B. Russel, J. Rheol. **24**, 287 (1980).
[24] P. Mazur and W. Van Saarlos, Physica A **115**, 21 (1982).
[25] W. Van Saarlos and P. Mazur, Physica A **120**, 77 (1983).
[26] J. F. Brady and G. Bossis, Annu. Rev. Fluid Mech. **20**, 111 (1988).
[27] J. M. Crowley, Phys. Fluids **19**, 1296 (1976).
[28] J. M. Crowley, Phys. Fluids **20**, 339 (1977).
[29] G. K. Batchelor and R. W. Janse van Rensburg, J. Fluid Mech. **166**, 379 (1986).
[30] B. Cichocki and B. U. Felderhof, Physica A **154**, 213 (1989).
[31] J. C. Bacri, C. Frenois, M. Hoyos, R. Perzynski, N. Rakotomalala, and D. Salin, Europhys. Lett. **2**, 123 (1986).
[32] J. F. Brady and L. J. Durlofsky, Phys. Fluids **31**, 717 (1988).
[33] M. Kardar, G. Parisi, and Y. Zhang, Phys. Rev. Lett. **56**, 889 (1986).
[34] E. Medina, T. Hwa, M. Kardar, and Y. C. Zhang, Phys. Rev. A **39**, 3053 (1989).
[35] J. G. Amar, P. M. Lam, and F. Family, Phys. Rev. A **43**, 4548 (1991).

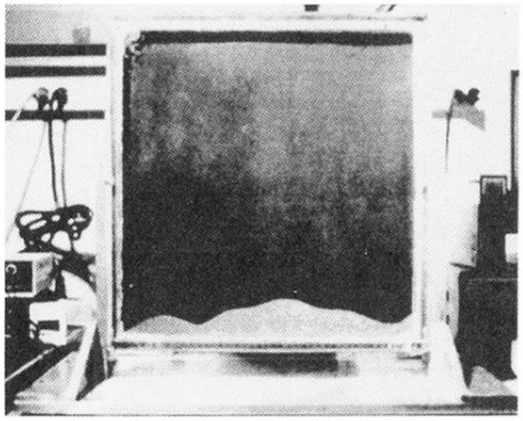

FIG. 1. Example of a typical cell with dimensions of 40×40 cm^2 and a cell gap of 1 mm.

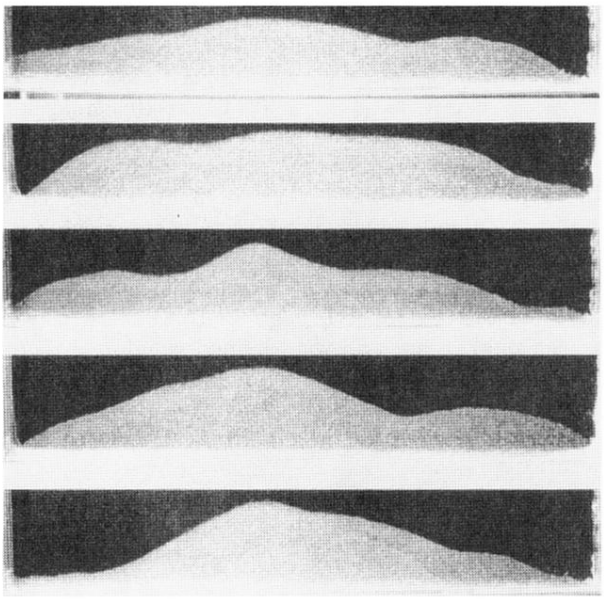

FIG. 2. Evolution of a typical initial configuration. Starting from the top picture, each picture shows the final interface after the cell is rotated once. The data shown are for cell type *A*.